Available online at www.sciencedirect.com
ScienceDirect
Thermochimica Acta 469 (2008) 77–85
thermochimica acta
www.elsevier.com/locate/tca

Kinetics of intermetallic phase formation in the Ti/Al multilayers

Emília Illeková [a,*], Jean-Claude Gachon [b], Alex Rogachev [c], Hamazasp Grigoryan [c], Julius Clemens Schuster [d], Anton Nosyrev [e], Petr Tsygankov [e]

[a] *Institute of Physics, Slovak Academy of Sciences, Dúbravska cesta 9, 845 11 Bratislava, Slovakia*
[b] *LCSM UMR7555, Université Henri Poicaré, 54506 Vandoeuvre les Nancy Cedex, France*
[c] *Institute of Structural Macrokinetics and Materials Science, RAS, 142432 Chernogolovka, Moscow, Russia*
[d] *Innovative Materials Group, Universität Wien, A-1090 Wien, Austria*
[e] *Bauman Moscow State Technical University, Moscow, Russia*

Received 18 July 2007; received in revised form 21 December 2007; accepted 26 December 2007
Available online 19 January 2008

Abstract

The kinetics of the synthesis of elemental nanoscaled multilayers of Ti and Al in the regime of continuous heating from 300 K up to 973 K was investigated. A series of sputter deposited Ti/Al multilayer thin films with individual layer thickness (d) from 4 nm up to 1000 nm have been used. Differential scanning calorimetry, Friedman–Gupta, Kissinger and Suriñach methods of complex kinetic analysis, classical and time resolved X-ray diffraction and scanning electron microscopy have been applied. In the Ti/Al multilayers the sequence of reactions leading to the final product TiAl (and Ti_3Al) is determined. The final products as well as the kinetics of their formation depend on the individual layer thickness. Three different kinetic regimes depending on the layer thicknesses have been found.

Keywords: Kinetics; Phase formation; Ti/Al multilayers; Nanofilms

1. Introduction

TiAl-based intermetallics due to their low specific weight, high specific strength, excellent creep strength and good oxidation resistance are promising materials for high temperature applications particularly in automotive and aerospace industries [1].

Recently it has been shown, that TiAl-based thin films can also be produced by suitable isothermal or continuous heating heat-treatment of Ti/Al multilayers produced by sputtering [2]. In such a case, due to the abnormally fast diffusion along grain boundaries in the individual layers and high exothermal effect, the intermetallics can also be formed after a specific thermal initiation by a self-propagating reaction in an autowave mode (combustion).

In order to develop the processing strategy it is necessary to study the kinetics of phase transformations in the Ti/Al system, to understand the growth mechanism, and both chemical and thermal stability of the produced titanium aluminides. The rapid phase evolution during the gasless combustion in the multilayer Ti/Al nanofilms can be studied by the time-resolved synchrotron radiation diffraction analysis (TRSRD) in [2–4]. The slow continuous heating controlled chemical reaction can also be followed by thermal analysis methods such as differential scanning calorimetry (DSC) or monitoring resistivity [5]. Recently, the peculiar relation between the specific thickness of the individual layers and the kinetics of the reaction at the Ti/Al interface has been observed [6] and the activation energies have been deduced. No relation between the combustion and continuous heating controlled reaction has been analyzed yet.

In the present paper, the complex kinetics of the formation of compounds in various Ti/Al multilayers, which should be controlled by the slow heating rate (up to 80 K min^{-1}), is studied in details for the first time. The role of the dimensions in the nano-layered system is analyzed.

2. Experimental

The multilayer foils were prepared by means of plasma-assisted magnetron sputtering. Details of the method were

* Corresponding author. Tel.: +421 2 5941 0526; fax: +421 2 5477 6085.
E-mail address: fyziille@savba.sk (E. Illeková).

0040-6031/$ – see front matter © 2008 Elsevier B.V. All rights reserved.
doi:10.1016/j.tca.2007.12.011

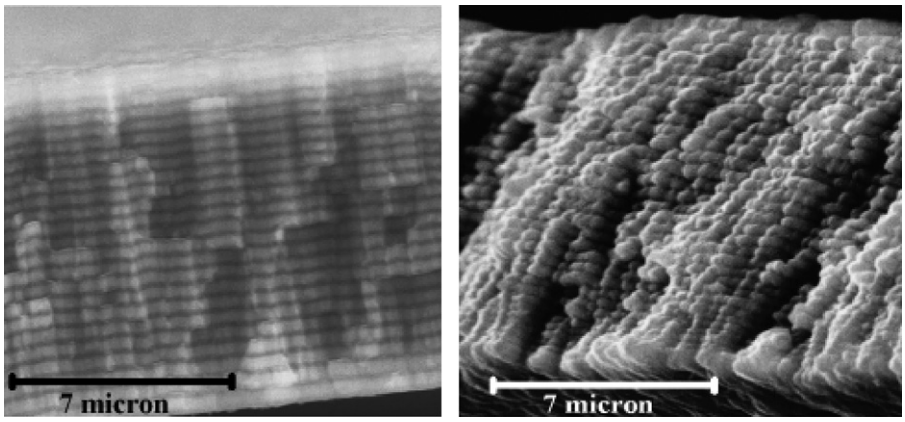

Fig. 1. SEM pictures of the initial multilayer foil with the layer thickness $d = 390$ nm (left) and the same sample after heating up to 973 K (right).

described in the earlier work [7,8]. Deposition procedure was based on simultaneous sputtering of two magnetron targets (Ti 99.9%, Al 99.99%) by low-energy ions (200 eV, up to 20 mA) in argon, at pressure 1–3 Pa. Up to 10 substrates of stainless steel foil or Si-wafer were placed circularly on the rotating holder. As the holder rotated, the substrates passed in turn through the fluxes of Ti and Al atoms from two different targets; therefore, alternating layers of these metals were created. Stepping motor provided rotating frequency in the range 0.03–20 rpm, which resulted in formation of individual layers with thickness, d, from 4 to 1000 nm. Deposition rate for each magnetron was established basing on volt–ampere characteristic for Ti and Al targets, and was controlled by micro-profile meter. Deposition chamber was preliminary pumped down to 10^{-4} Pa with turbo-molecular pump. Substrate temperature was kept below 323 K in order to prevent diffusion and reaction during deposition. The samples with stoichiometric ratio Ti/Al were prepared. In each multilayer, the thickness of individual Ti layer and Al layers was practically equal (within the range of experimental error), therefore we can assume approximately $d_{Ti} = d_{Al} = d$ (and the bilayer thickness $\Lambda = 2d$). A set of multilayers has been prepared, where the number of individual layers is varying from 20 to 5000. However, total thickness of each foil is always 18–20 μm.

As-deposited reactive multilayer foils (RMF) were separated from substrates and the reaction under the condition of slow continuous heating was studied. A small amount (1–4 mg) of the RMF was placed in a platinum crucible, loosely covered (without restraint) by the platinum lid and heated at the constant heating rate, β, being 5–80 K min^{-1} under flowing argon atmosphere (20 ml min^{-1}) in a power-compensation differential scanning calorimeter (Perkin-Elmer DSC-7). For comparison, DSC experiments at 10 K/min were performed utilizing a Setaram DSC111 calorimeter. The kinetics of chemical reactions was studied within the temperature range 300–973 K. The absolute temperature (error less than 0.5 K) and the enthalpy (error less than 2 J g^{-1}) of the DSC instrument were calibrated for all heating rates.

The mechanical quality of the as-prepared Ti/Al foils samples varies with the thickness of the individual layers, thus whereas foils with $d = 1000$ nm are very brittle and disintegrate during sample cutting into smaller pieces, called “brash”, foils with thinner layers are suitably strong. In any case, the small strips of the multilayered foils are slightly deformed after being cut-off and the thinner the layers the more they twist due to the formation of new phases and they even lift up the sample pan-lid in the course of the DSC heat-treatment. Those movements have been reflected in increased noise in the thermograms and numerous irreproducible kinks especially in the course of the peaks.

The samples were tested with scanning electron microscopy equipped with energy dispersive X-ray spectroscopy (SEM/EDX) and X-ray diffraction (XRD) analyses. Data of time-resolved synchrotron radiation diffraction analysis (TRSRD) were also used for identification of phases appearing during the reaction. Examples of the initial sample microstructures and of the late, i.e. before and after the DSC measurements, are shown in Fig. 1. When the thickness of individual layer exceeds 100 nm, layered structure persists after reaction, as illustrated by Fig. 1. Existence of fine rounded grains within each layer becomes more evident in the reaction product. Microstructure features of the reaction products in the Ti/Al foils with layer thickness less than 20 nm are not clear up-to-date. Preparation of the reacted foils for TEM faces difficulties because of brittleness of the reacted foils, while SEM cannot provide high enough resolution. Thus, transformations of the layer microstructure during reaction in the thin-layer foils represent a task for future experimental work.

3. Results

3.1. Differential scanning calorimetry

The thermogram in Fig. 2 shows that the sequence of three transformations ($R1 + R2$ at 650–850 K and $R3$ at 900–1000 K) occurs in the samples with thick enough layers. Data obtained with Perkin-Elmer DSC-7, presented in Fig. 3, show that reactivity of Ti/Al multilayers increases with decreasing individual layer thickness (d), and that both heat effects and kinetics of irreversible transformations in the samples depend on d. The effect $R1$ is closely followed with $R2$, so they form one broad and large exothermal double-peak (Figs. 2 and 3). Decreasing d results in increasing significance of low-temperature stages of

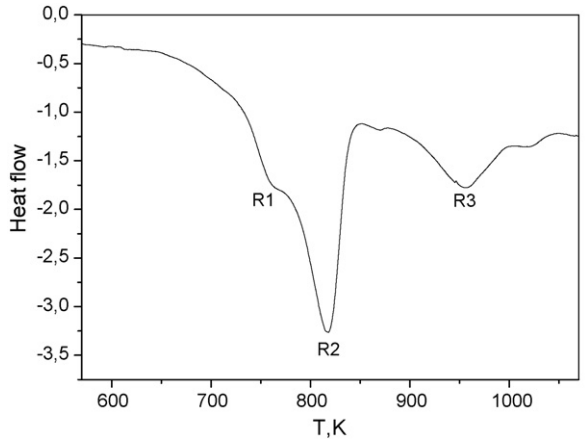

Fig. 2. Thermogram obtained by Setaram DSC 111 for the sample with layer thickness $d = 390$ nm, heating rate 10 K/min.

the reaction in the range 1000–20 nm. Samples with $d = 4$ nm exhibit a different behavior, the major exothermal peak drifts toward higher temperature.

In addition to the size effect, which takes place in the extremely thin layers (mentioned above), we have obtained some indication about the role of the outer surfaces of the individual stripes of RMF, too. Namely, the intact strips and brash samples in the case of the thickest layers, $d = 1000$ nm, gave two different types of thermograms systematically reflecting the inequality in the rate controlling factor (Fig. 4a). In further analysis, we focus mainly on the results for intact strip samples.

In the case of the very thick layers, i.e. in samples with $d = 1000$ nm, no individual $R3$ transformation step has been observed with Perkin-Elmer DSC-7 (Fig. 4a) probably due to the fact that the primary transformation steps $R1 + R2$ proceed at higher temperatures, and, at the same time, DSC-7 is limited to 973 K. All three steps are observed in the samples with

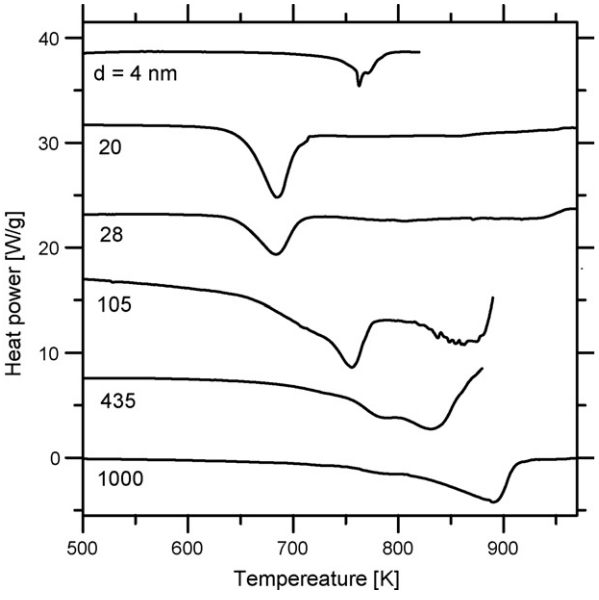

Fig. 3. Continuous heating DSC signal of various as-prepared Ti/Al multilayers at 40 K min^{-1} heating rate. The thickness of the individual layers in each multilayer is the parameter.

$d = 105$ nm, as shown in Fig. 4b. Further decreasing of layer thickness down to 28 nm leads to disappearance of one of the lower-temperature peaks (see Figs. 3 and 4c). Samples with layer thickness equal to 4 nm react within the temperature range 700–800 K. In all samples, the final product of these reactions is $TiAl + Ti_3Al$. The relative amounts of these two phases vary only a little and in a non-systematic mode. Fig. 5a and b show examples of the XRD powder patterns obtained.

3.2. Kinetic analysis

General aim of any kinetic analysis is the description of the progress of a transformation. In the case of the solid-state reactions (or transformations) due to the fact that not only one mechanism (as diffusion or interface reaction) might participate and several intermediate states might bypass, all of which can have different temperature dependences, the analytical studies need to be simplified. Thus it is being assumed [9] that the considered reaction rate $d\alpha/dt$ is the product of one independent kinetic function, $f(\alpha)$, which is dependent solely on the fraction transformed (or the dimensionless degree of conversion), α, and the function $k(T)$, which follows only an Arrhenius-type temperature dependence.

$$\frac{d\alpha}{dt} = f(\alpha)k(T), \tag{1}$$

$$k(T) = A \exp\left[\frac{-E^*}{RT}\right], \tag{2}$$

where A and E^* are kinetic parameters of the transformation that are independent of the measuring regime and R is the universal gas constant. For non-isothermal experiments, $d\alpha/dt$ at all times depends on both $f(\alpha)$ and $k(T)$, and the determination of $f(\alpha)$, A and E^* is an interlinked problem. Thus in this paper, we firstly perform the analysis of the activation energy, E^*, without invoking any kinetic model. Then we try to determine the proper kinetic function, $f(\alpha)$, by fitting the known theoretical kinetic functions to our data.

3.3. Activation energy

Concerning the determination of E^* the model-free isoconversional methods effectively test the constancy $E^* \neq E^*(\alpha)$, e.g. [10–12]. The one basic assumption of these methods is that $f(\alpha)$ is independent of the measuring regime, i.e. of β in the case of continuous heating experiments. Then, the simple relation between the appropriate measured quantity $p(\alpha_{fix},\beta)$ and the temperature $T_{\alpha fix,\beta}$ at various heating rates, β, characterizing the equivalent stage of the reaction (also called fixed stage), α_{fix}, determines the wished $E^*(\alpha_{fix})$. On the other side, each unique data point of $E^*(\alpha_{fix})$ responding to the wished constant α convolves the complex information of all measured dependencies (all thermograms at various β in our case) and from the whole thermograms (to identify each $\alpha = \alpha_{fix}$). The accuracy of various model-free isoconfigurational methods has been analyzed by Starink [13]. In the case of continuous heating measuring regime, six sources of errors have been assessed. In the case of the Perkin-Elmer

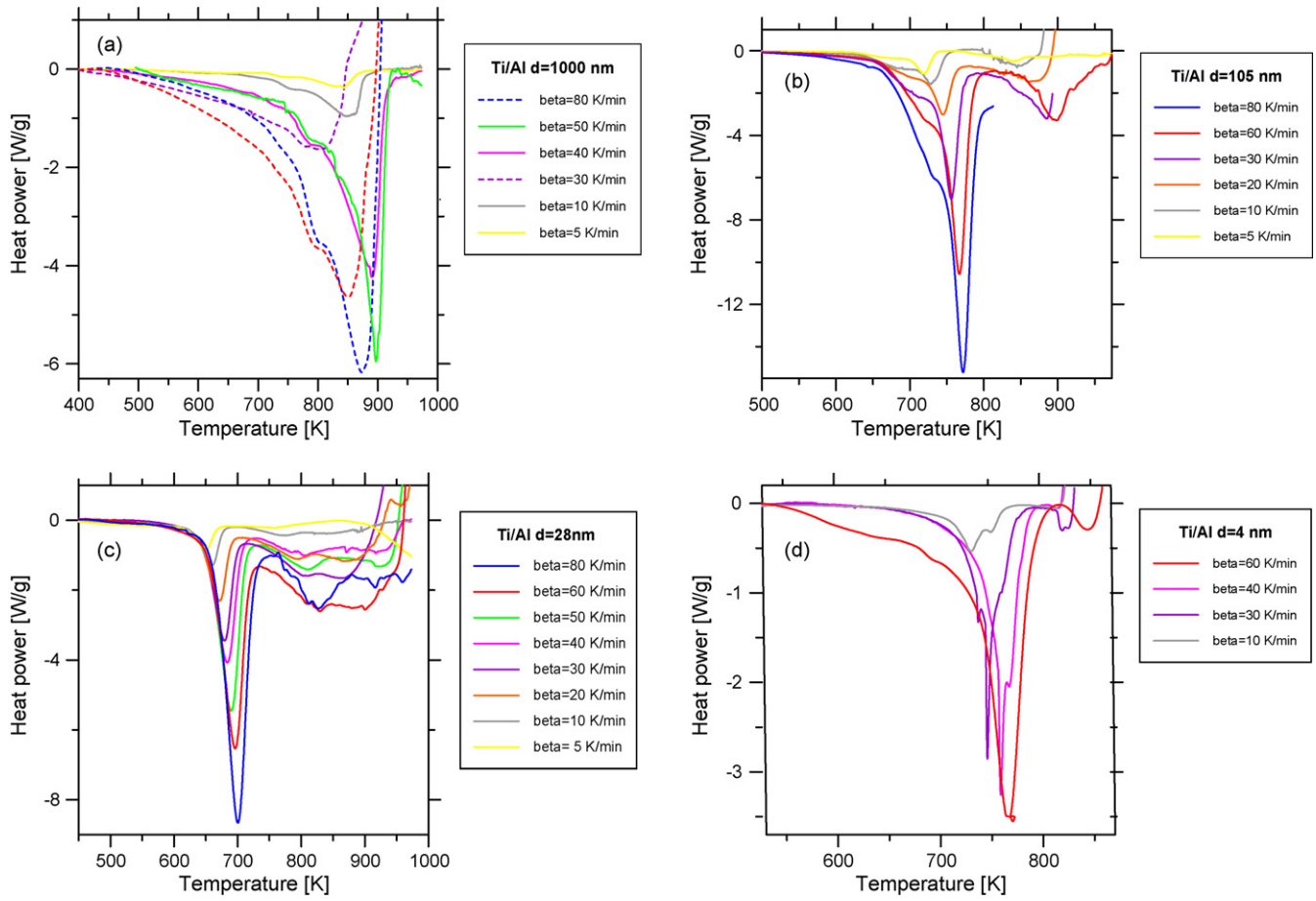

Fig. 4. (a) Two types of heating rate dependencies of the DSC traces for the as-prepared Ti/Al multilayer with $d = 1000$ nm. Full-line curves are for intact strip samples; dashed-line curves are for brash samples. (b) Heating rate dependence of the DSC traces for the as-prepared Ti/Al multilayer with $d = 105$ nm. (c) Heating rate dependence of the DSC traces for the as-prepared Ti/Al multilayer with $d = 28$ nm. (d) Examples of the DSC thermograms at different heating rates for the as-prepared Ti/Al multilayer with $d = 4$ nm.

DSC, the actual temperature regime (the constant $\beta = \mathrm{d}T/\mathrm{d}t$) is not directly measured, being predetermined. In the investigated reactions in the Ti/Al multilayers, which are seen in Fig. 3, the transformation heats are large, they vary between 640 and 300 J g^{-1} decreasing to ~100 J g^{-1} for $d = 4.5$ nm. However, due to the very good heat exchange between the small and very thin metallic strips and the surroundings, these two potential inaccuracies are insignificant, as also has been recognized from the sigmoidal shape of each $\alpha(T)$ dependence, see e.g. Fig. 6, or as will be confirmed later by the curve fitting. Because our power-compensation DSC is measuring exactly $\mathrm{d}\alpha/\mathrm{d}T$ [14], we decided to use the differential isoconversional Friedman–Gupta method [15,16]

$$\ln\left(\frac{\mathrm{d}\alpha}{\mathrm{d}T}\beta\right)_{\alpha_{\mathrm{fix}}} = -\frac{E^*(\alpha_{\mathrm{fix}})}{RT_{\alpha_{\mathrm{fix}}}} - \ln f(\alpha_{\mathrm{fix}}). \quad (3)$$

In this case, excepting the noise of the DSC signal, which represents the non-systematic errors, the temperature dependence of the equilibrium state being the baseline for each individual DSC peak is the only source of inaccuracies [13]. In our calculations, we received the best results approximating the baselines by the third power polynomials.

As is seen in Fig. 7a, in the case of Ti/Al multilayers with $d = 28$ or 20 nm, E^* systematically slightly decreases with increasing α. If $d \geq 105$ nm, the $E^*(\alpha)$ dependence is much more complicated and the error bars are larger than 12 kJ mol^{-1} as is seen in Fig. 7b. These results are not surprising because these $E^*(\alpha)$ dependencies represent single-peaks in the DSC experiments in the case (a) and double-peaks, ($R1 + R2$), in the case (b). However, they are important, because they provide evidence of the constant reaction mechanism in the case (a) and of changes in the reaction mechanism, which are associated with changes in the activation energy in the case (b).

As it has been indicated above, due to the multi-step nature of the investigated synthesis in the Ti/Al multilayers, the numerical values of E^*_{α} have no physical meaning. Also due to the variability in the individual $E^*(\alpha)$ dependencies for various individual foils, the eventual dependence of the effective activation energy on the thickness of the individual layers, $E^*(d)$, is hard to discuss. Taking this into account, we have used an elementary and rapid isoconversional method namely the integral generalized Kissinger method

$$\ln\frac{\beta}{T^2_{\alpha_{\mathrm{fix}}}} = \frac{-E^*}{RT_{\alpha_{\mathrm{fix}}}} + C. \quad (4)$$

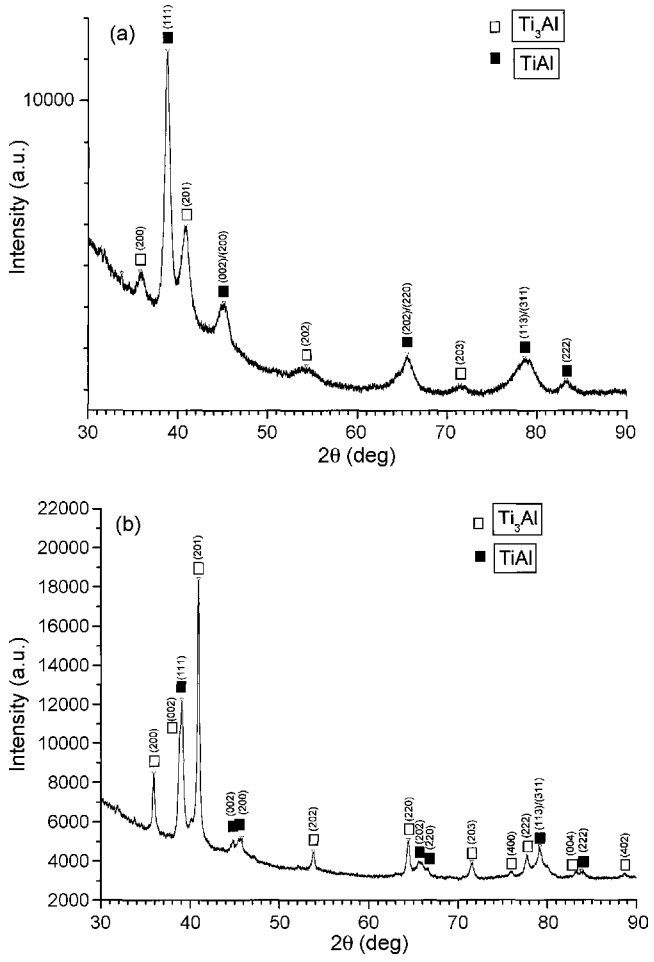

Fig. 5. (a) XRD powder pattern of the Ti/Al multilayer with $d = 20$ nm after its DSC heat-treatment up to 973 K at the heating rate 40 K min^{-1}. Majority phase: TiAl, minority phase: Ti_3Al. (b) XRD powder pattern of the Ti/Al multilayer with $d = 435$ nm after its DSC heat-treatment up to 973 K at the heating rate 20 K min^{-1}. Majority phase: Ti_3Al, minority phase: TiAl.

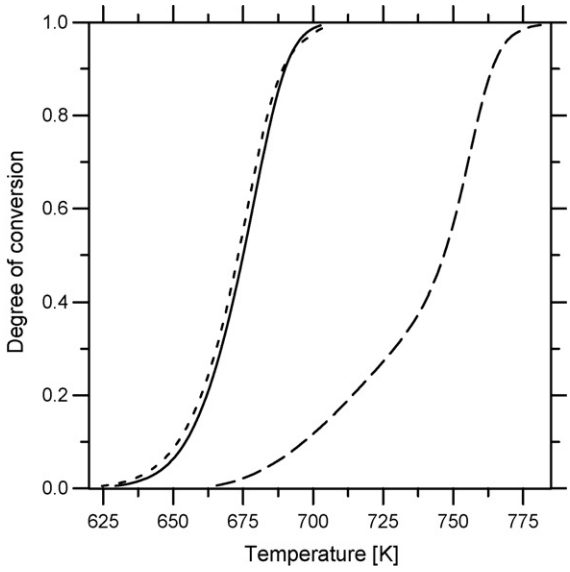

Fig. 6. Degree of conversion versus temperature representation of the DSC data at the heating rate 30 K min^{-1} for the synthesis in Ti/Al multilayers with $d = 20$ nm (short dashed line), $d = 28$ nm (full line) indicating one transformation step and $d = 105$ nm (large dashed line) indicating the superposition of two elementary transformations.

In several papers [17,13] the validity of this method has been investigated, concluding that the only condition, namely that the $T_{\alpha,\mathrm{fix}}$ corresponds to the same degree of conversion $\alpha = \alpha_{\mathrm{fix}}$ for all heating rates, β, must be satisfied. We have calculated the apparent activation energies at the moments of the maximum of dα/dT for all individual foils, E^*_{K}, as the slopes of the so called Kissinger dependencies of $\ln(\beta/T_{\mathrm{p}})$ versus $1/RT_{\mathrm{p}}$, when $T_{\alpha,\mathrm{fix}} = T_{\mathrm{p}}$ is the temperature of the DSC peak [17]. We have established that, for the considered foils, always only a small variation in the degree of conversion at the maximum reaction rate with heating rate occurs, namely $\alpha_{\max} = 0.622 \pm 0.001$ if $d = 28$ nm or the overall $\alpha_{\max} = 0.72 \pm 0.02$ if $d = 105$ nm. Also we have found that taking the data from the heating rates 5–80 K min^{-1}, the Kissinger plots for all Ti/Al multilayers stay on straight lines. Thus for example in Fig. 8a, the Kissinger plot for the sample with $d = 28$ nm gives $E^* = 192 \pm 7$ kJ mol^{-1}. However, the Kissinger plot for the sample with $d = 1000$ nm indeed follows two different straight lines, which are shown in Fig. 8b, namely one for larger fragments ($E^*_{\mathrm{K}} = 233 \pm 34$ kJ mol^{-1}) and another one indicating substantially smaller activation energy ($E^*_{\mathrm{K}} = 109 \pm 14$ kJ mol^{-1}) for the brash samples. The Kissinger straight line fit with low correlation coefficient $c = 0.95$ ($E^*_{\mathrm{K}} = 220 \pm 15$ kJ mol^{-1}) has been obtained only from the noisy peaks of samples with $d = 4$ nm. Summary of all E^*_{K} is presented in Table 1.

Summarizing the previous paragraphs, the difference in activation energies determined by the Kissinger method and the Friedman–Gupta method, which does not exceed 10%, has been obtained. Similar deviations have, for example, been achieved for the cold crystallization of Fe–Si–B metallic ribbons [10] or for the thermal dehydration of calcium oxalate monohydrate [18]. Generally, integral isoconversional methods may give rise to noticeable systematic errors in E^* when the latter strongly varies with α [13,18]. In any case, for the synthesis in the Ti/Al multilayers, it is evident that the E^* of the samples with $d = 20$ or 28 nm is much less than that for the samples with thicker layers. This result is in a good agreement with the data of Ramos et al. [19]. For the sample with $d = 20$ nm, the calculated ΔE^*_{K} is matching the activation energy reported for $TiAl_3$ formation in Ti/Al diffusion couples [20]. For samples with larger layer thickness the respective values are higher.

Table 1
Relation between the thickness of individual layers and the apparent activation energy of the new phase formation in the as-prepared Ti/Al multilayers during the continuous heating in DSC

Thickness of the individual layer, d (nm)	ΔE^*_{K} (kJ/mol)
1000	233 ± 34
435	244 ± 6
105	218 ± 9
28	192 ± 7
20	169 ± 3
4	220 ± 15

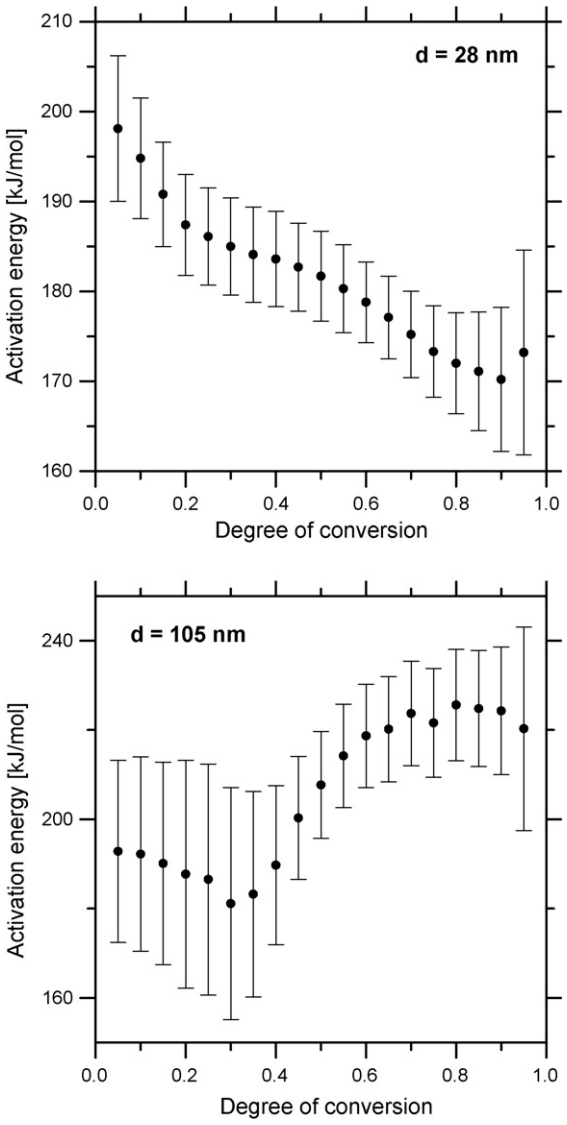

Fig. 7. Effective activation energy as a function of total degree of conversion for continuous heating in DSC synthesis in Ti/Al multilayers with (a) $d = 28$ nm and (b) $d = 105$ nm.

3.4. Kinetic model

As it has been shown by the DSC measurements, the shape of the first massive exotherm varies with the thickness of individual layers, d. It reveals two transformation steps $R1$ and $R2$ in some cases, however it is not dependent on the experimental heating rate, β, in the case of Ti/Al multilayers. In such case the Suriñach curve fitting procedure [21,22] might help to specify the complex kinetic character of those transformation steps. Namely, each single DSC curve, represented in an appropriate coordinate system

$$\ln\left[\frac{\mathrm{d}\alpha(T,t)}{\mathrm{d}T}\right] + \frac{E^*}{RT(t)} + \ln\,\beta \;\text{versus}\; -\ln[1-\alpha(T,t)] \qquad (5)$$

is compared with the theoretical model ones. The advantage of this routine is that the theoretical Suriñach plots for different hypothetical kinetics that might participate in any solid-state sample [9] differ from each other in a principal way (see Fig. 9). Thus, the kinetics which are controlled by any diffusion are represented by the appropriate Suriñach plots which are concave curves. The Johnson–Mehl–Avrami (JMA) nucleation-and-growth kinetics

$$\left(\frac{\mathrm{d}\alpha}{\mathrm{d}t}\right) = \frac{1}{\tau}n(1-\alpha)[-\ln(1-\alpha)]^{n-1/n} \qquad (6)$$

with an Avrami exponent $n > 1$ follow the appropriate convex curves and the nth order reactions (not shown) or also the normal-grain-growth processes [23] follow the Suriñach straight lines.

In the case of Ti/Al multilayers, all thermograms taken at each heating rate have been used. Firstly, the individual $E^*(\alpha)$ dependencies were neglected and only the apparent activation energies E^*_K were used in Eq. (5). In such case, for smaller d being 20 nm or 28 nm, the Suriñach plots correspond reasonably well to the JMA kinetics with $n = 1.5$–1.3 during the whole transformation when n slightly decreases with increasing α for all β (Fig. 10a). Afterwards, another effective activation energy, as for example $E^* = 172$ kJ mol^{-1} being the lowest one in the $E^*(\alpha)$ dependence

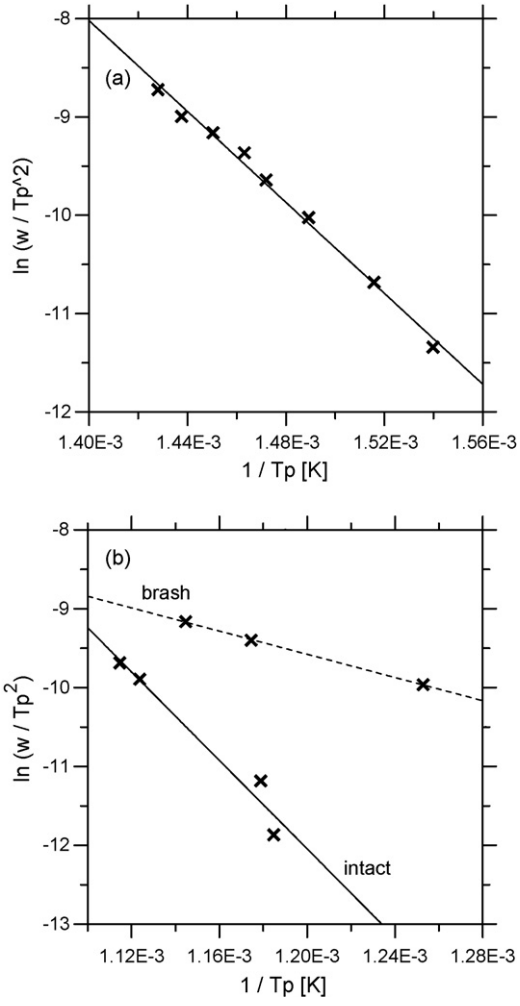

Fig. 8. (a) Kissinger plot for the main transformation step in as-prepared Ti/Al multilayer with $d = 28$ nm. (b) Kissinger plots for the principal transformation step in as-prepared Ti/Al multilayer with $d = 1000$ nm. Full-line curve fits the dates for intact strip samples; dashed-line curve is for brash samples.

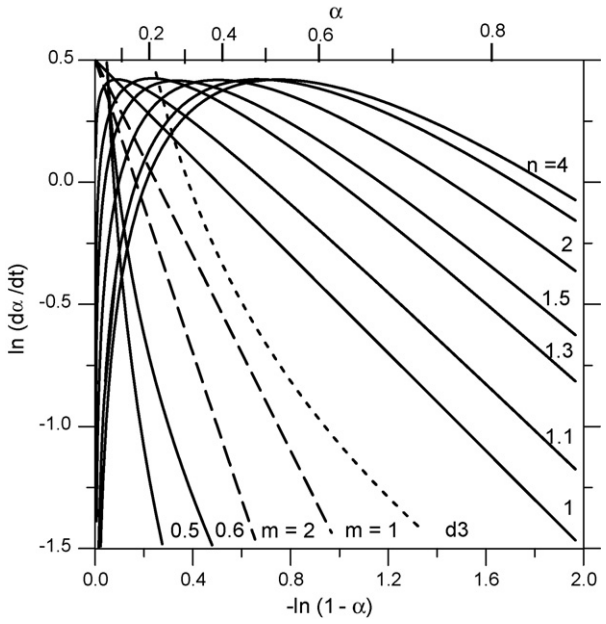

Fig. 9. Suriñach plots for different theoretical kinetic functions. Full lines correspond to the Johnson–Mehl–Avrami (JMA) nucleation-and-growth kinetics [9], exponent n being the parameter. Dashed lines correspond to the normal-grain-growth kinetics [23], exponent m being the parameter. The dotted line corresponds to the long-range diffusion kinetics [9]. JMA model lines are vertically shifted to show the maxims at the same level.

from Fig. 7a, was used instead. Such modified Suriñach plot is also shown in Fig. 10a. Also in this case the JMA kinetics is evident, just n is slightly higher. In the advanced stages of the reaction, the difference between these two computed curves is of the order of the difference between the previously computed experimental and the theoretical Suriñach curve. As the consequence of this quantitative assessment, the observed decrease in $n(\alpha)$, assuming fixed E^*, will become constant $n = 1.5$ due to the true decreasing $E^*(\alpha)$ dependence.

For larger d, such as 105 nm or 435 nm, and $E^* = E^*_K$, the Suriñach plots of the $R1 + R2$ double peak, again stay on one master curve for all β (Fig. 10b). This master curve follows the theoretical JMA kinetics with $n = 0.5$ at the beginning. Then the kinetics dramatically changes (as it already has been predicted from the true $E^*(\alpha)$ analysis). Finally the master curve follows the theoretical JMA kinetics with $n = 1.5$. Changing the fixed $E^*_K = 218\,\mathrm{kJ\,mol^{-1}}$ for $E^* = 180\,\mathrm{kJ\,mol^{-1}}$, which is the lowest possible value deduced from the true $E^*(\alpha)$ dependence shown in Fig. 7b, the principal character of the master curve does not change neither in the early nor in the advanced stages excepting its vertical shift. Finally, the coincidence between the parts of the master curve and the particular theoretical Suriñach curves gives the indication that only the $R1$ transformation step takes place at the early stages of the $R1 + R2$ reaction (if $\alpha < 0.3$ and $d = 105$ nm or if $\alpha < 0.45$ and $d = 435$ nm); and only $R2$ transformation step takes place at the end (if $\alpha > 0.7$) for both samples. Thus, the JMA kinetics and the Avrami exponents $n_1 = 0.5$ and $n_2 = 1.5$ have been deduced for the $R1$ and the $R2$ transformation steps for both samples.

In the case of the RMF with $d = 1000$ nm, two types of thermograms obtained (Fig. 4a) have been represented by two individual Suriñach plots (not shown). Thus for the samples of block fragments the JMA kinetics with $n_1 = 0.5$ for $\alpha \leq 0.2$ and $n_2 \sim 1.1$–1.5 for $\alpha > 0.75$ has been deduced. However, in the case of the brash samples, the apparent JMA kinetics with $n_1 < 0.5$ for $\alpha \leq 0.2$ later continuously changes. Therefore we suppose that in this case the early stages of the synthesis might even be controlled by the long-range diffusion for $\alpha > 0.3$.

In the Ti/Al multilayer with $d = 4$ nm, the principal transformation exotherm (probably a new type, as follows from Figs. 1 and 3) is deformed entirely in its central part at each

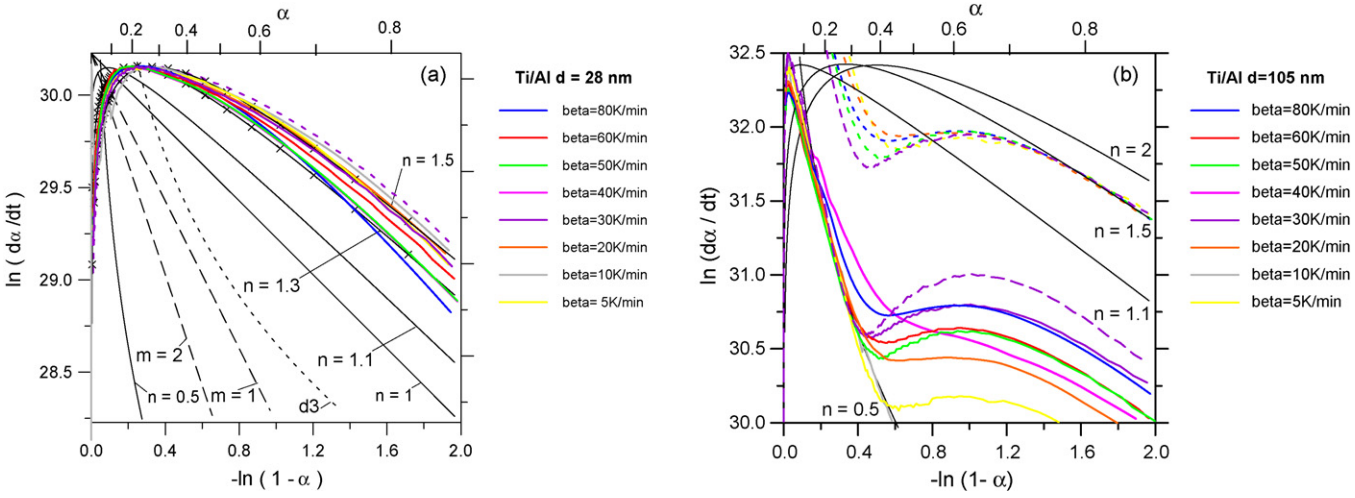

Fig. 10. (a) Suriñach representations of the continuous heating DSC curves from Fig. 4c for the new phase formation in the as-prepared Ti/Al multilayer with $d = 28$ nm if $E^* = 192\,\mathrm{kJ\,mol^{-1}}$. The dashed line represents the DSC measurement if $E^* = 172\,\mathrm{kJ\,mol^{-1}}$. The curves are shifted vertically to show the maxima at the same level. The black lines represent the same theoretical kinetic functions as in Fig. 9, symbols (x) highlight the theoretical lines for the JMA kinetics with $n = 1.5$ and 1.3. (b) Suriñach representations of the continuous heating DSC curves from Fig. 4b for the new phase formation in the as-prepared Ti/Al multilayer with $d = 105$ nm if $E^* = 218\,\mathrm{kJ\,mol^{-1}}$. The large-dashed line represents the DSC measurement if $E^* = 190\,\mathrm{kJ\,mol^{-1}}$. The curves for various heating rates are shifted vertically to show the kinetics of the $R1$ transformation step (full lines). Short-dashed lines are the same curves shifted up vertically to show the kinetics of the $R2$ transformation step. Thin black lines are the plots for the theoretical JMA kinetics with $n = 0.5$, 1.1, 1.5 and 2.

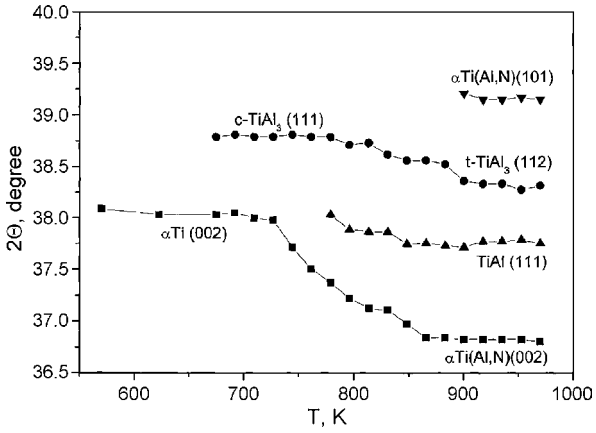

Fig. 11. Evolution of angular position of the major TSRSD peaks for titanium aluminides starting with metastable c-$TiAl_3$ and ending with TiAl for Ti/Al multilayer with $d = 390$ nm continuously heated with the heating rate of 10 K min^{-1}. The peak initially being at $2\theta = 38.0$ yields a c-parameter smaller than for pure α-Ti, indicative of nitrogen in the solid solution. The peak at $2\theta = 39.15$ yields an a-parameter smaller than for pure α-Ti, indicative of Al in solid solution. Thus, the α-Ti(Al,N) phase has been labeled.

β (Fig. 4d) indicating more complex kinetics and mechanisms. Incidentally, no ideal Suriñach curve could be found for this case and interpreted. In this case, the Suriñach curves are distorted and they reflect no reproducible physical sense up to high degree of conversion; finally they follow the JMA kinetics with $n = 1$ for $\alpha > 0.7$.

4. Discussion

As has already been well established, in multilayer films the first stage of intermediate phase formation is the nucleation of an amorphous phase [5]. Our TRSRSD results in Fig. 11 manifest that the first crystalline phase to be formed in Ti/Al massive diffusion couples is $TiAl_3$ [20]. In the case of $d = 20$ nm, the kinetics results have shown exactly the activation energy reported for this phase. However, the results of the XRD analysis present TiAl and some Ti_3Al to be the final products of the reaction(s) (Fig. 5a and b). This apparent discrepancy can also be reconciled with the TRSRD data. Fig. 11 shows the appearance of initially (metastable) cubic $TiAl_3$, which then gradually changes to stable tetragonal $TiAl_3$, then $TiAl_2$, and finally TiAl in the sample with $d = 390$ nm. This yields in fact a series of peaks, which are not well separated in the DSC scan.

We suppose, that for most multilayer samples amorphisation is not complete before nucleation of the first crystalline phase does start. In samples with thin layers, the relatively large area of interface between the starting phase(s) and the amorphous phase provide many nucleation sites for the first intermediate phase to crystallize (Fig. 12, center). Thus the heterogeneous nucleation is not rate limiting and the DSC peak observed in samples with $d = 20$ and 28 nm is due to the crystal growth. This is characterized by low activation energy and exponent $n = 1.5$. For samples with larger layer thickness there are less interfaces and thus less sites for the heterogeneous nucleation available for the crystallization of $TiAl_3$ (Fig. 12, left). Thus, nucleation increasingly becomes the dominant (rate limiting) effect for a sequence of two separate transformation steps $R1 + R2$. After an initial nucleation event (exponent $n_1 = 0.5$ for the $R1$ DSC peak) the second DSC peak is found to be compatible with three-dimensional crystal growth having higher activation energy and exponent $n_2 = 1.5$.

This model offers a natural interpretation of the behavior of the sample with extremely thin layers. In this case, all starting

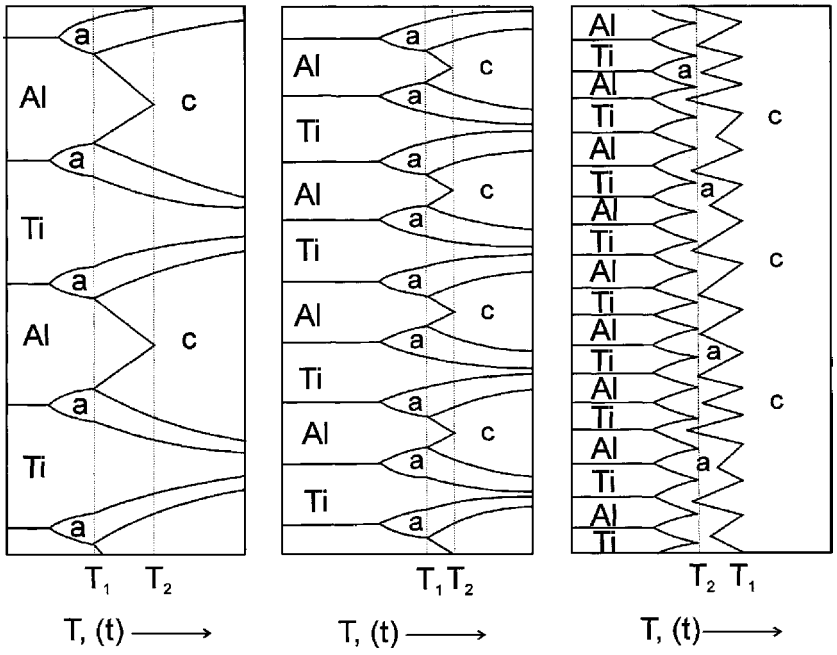

Fig. 12. Schematic evolution of phase formation in Al–Ti multilayers: For thick layers (left) the temperature T_1 of nucleation of the crystalline c-$TiAl_3$ phase (c) is well separated from the temperature of the disappearance T_2 of the Al-crystals providing the nucleation sites. For thinner layers, $20 \leq d \leq 28$ nm, (center) T_2 moves close to T_1, and for very thin layers (right) T_2 occurs before T_1, which causes substantially delayed nucleation of any crystalline phase from amorphous phase (a).

material becomes amorphous before any crystalline phase can nucleate (Fig. 12, right). Thus the start of the crystallization is delayed. The DSC peak of the sample with layer thickness of only $d = 4$ nm is shifted to higher temperatures and the irregularities of this peak indicate competition of several types of nucleation such as impurity nucleation (e.g. at the wall of the sample container) or even homogeneous nucleation.

Therefore we can propose the following mechanism of the process: In Ti-Al multilayer samples with layer thickness of 20 nm or more, the same reaction sequence for the formation of intermediate phases is observed. It starts with amorphisation and ends with the formation of TiAl. The kinetics is controlled by the nucleation of the metastable c-$TiAl_3$ phase. For larger layers thickness, few nucleation sites are available and it takes time until the crystals of the newly formed phase grow to sizes large enough to provide substantial heat effects. Thus, nucleation and crystal growth are separated. For thinner layers the interface between the amorphous phase and the starting materials (Ti, Al) is larger and the large number of available nucleation sites corresponds to a large number of nuclei. Their growth forms the DSC peak already at lower temperatures. In the samples with very thin layers, the whole starting material is amorphized before the crystallization of an intermediate phase starts. Because no sites for heterogeneous nucleation are left nucleation is inhibited. This causes a shift of the thermal effect in the DSC towards a higher temperature.

5. Conclusions

Summarizing the results of the complex kinetic analysis, including the character of the DSC thermograms, their Suriñach analyses and Kissinger plots, and taking into account XRD, TRSRD and SEM data concerning phase constitution of the samples, the following conclusions can be expressed:

In Ti/Al multilayers, the synthesis between Ti and Al, when is controlled by slow heating rate (in DSC), proceeds below 973 K. This synthesis being a complex reaction is a sequence of gradual changes. The final products are TiAl and Ti_3Al; they are independent of the thickness of the individual layers, d. However, the rate limiting process is the nucleation and growth of the intermediate $TiAl_3$ phase. The observed $R1$ transformation step is the heterogeneous nucleation of $TiAl_3$ (JMA kinetics, $n_1 = 0.5$, $E^*_1 < E^*_2$). $TiAl_3$ nucleates heterogeneously at the amorphous/Al interface. $TiAl_3$ does not nucleate heterogeneously in the amorphous phase. The observed $R2$ transformation step is the three dimensional diffusion controlled growth of $TiAl_3$ (JMA kinetics, $T_{p2} = T(d)$, $n_2 = 1.5$, $E^*_2 = E^*(d)$). Two size effects limiting this scheme have been identified (for $d \sim 4$ nm and for sample dimensions of the order of thickness of the multilayer).

Acknowledgements

We acknowledge financial support of INTAS (grant 03-51-4103), VEGA (grant 2/5096/25), APVV-0413-06, SAS Center of Excellence NANOSMART, RFBR (grant 04-03-32654) and joint CNRS-RFBR (French-Russian project).

References

[1] D.M. Dimiduk, Mater. Sci. Eng. A263 (1999) 281–288.
[2] J.-C. Gachon, A.S. Rogachev, H.E. Grigoryan, E.V. Illarionova, J.-J. Kuntz, D. Yu. Kovalev, A.N. Nosyrev, N.V. Sachkova, P.A. Tsygankov, Acta Mater. 53 (2005) 1225–1231.
[3] A.S. Rogachev, J.-C. Gachon, H.E. Grigoryan, A.N. Nosyrev, P.A. Tsygankov, J.C. Schuster, D. Vrel, Nucl. Instr. Methods Phys. Res. A 543 (2005) 175–179.
[4] A.S. Rogachev, J.-C. Gachon, H.E. Grigoryan, E. Illeková, N.F. Kochetov, F.N. Nosyrev, N.V. Sachkova, J.C. Schuster, M.R. Sharafutdinov, N.F. Shkodich, B.P. Tolochko, P.A. Tsygankov, I.Y. Yagubova, Nucl. Instr. Methods Phys. Res. A 575 (2007) 126–129.
[5] R.B. Schwarz, J.B. Rubin, J. Alloys Comp. 194 (1993) 189–197.
[6] A.S. Ramos, R. Calinas, M.T. Vieira, Surf. Coat. Technol. 200 (2006) 6196–6200.
[7] A.E. Grigoryan, N.G. Elistratov, D.Yu. Kovalev, A.G. Merzhanov, A.N. Nosyrev, V.I. Ponomarev, A.S. Rogachev, V.I. Khvesyuk, P.A. Tsygankov, Dokl. Akad. Nauk. 381 (2001) 368.
[8] N.G. Elistratov, A.N. Nosyrev, V.I. Khvesyuk, P.A. Tsygankov, Appl. Phys. (Russ.) 3 (2001) 8.
[9] J. Šesták, Měření termofyzikálních vlastností pevných látek, Teoretická termická analýza, Academia, Praha, 1982, pp. 140–170 and 316–317 (or J. Šesták, Thermophysical Properties of Solids—Their Measurements and Theoretical Thermal Analysis, Academia Prague, Prague, 1984).
[10] E. Illeková, I. Mat'ko, P. Duhaj, F.A. Kuhnast, J. Mater. Sci. 32 (1997) 4645–4654.
[11] E. Illeková, Doctoral dissertation, Ministery of Education, Slovakia, Comenius University, Bratislava, Institute of Physics, SAS, Bratislava, 2005, pp. 1–69.
[12] S. Vyazovkin, I. Dranca, Macromol. Chem. Phys. 207 (2006) 20–25.
[13] M.J. Starink, Thermochim. Acta 404 (2003) 163–176.
[14] E. Illeková, B. Aba, F.A. Kuhnast, Thermochim. Acta 195 (1992) 195–209.
[15] H.L. Friedman, J. Polym. Sci. C6 (1964) 183.
[16] A.K. Gupta, A.K. Jena, M.C. Chaturvedi, Scr. Metall. 22 (1988) 369.
[17] H.E. Kissinger, Anal. Chem. 29 (1957) 1702–1706.
[18] S. Vyazovkin, J. Comput. Chem. 22 (2001) 178–183.
[19] A.S. Ramos, M.T. Vieira, Surf. Coat. Technol. 200 (2005) 326–329.
[20] F.J.J. van Loo, G.D. Rieck, Acta Metall. 21 (1973) 61–71.
[21] S. Suriñach, M.D. Baró, M.T. Clavaguera-Mora, N. Clavaguera, J. Non-Cryst. Solids 58 (1983) 209–217.
[22] E. Illeková, Thermochim. Acta 280/281 (1996) 289–301.
[23] E. Illeková, in: B. Idzikowski, P. Švec, M. Miglierini (Eds.), Properties and Applications of Nanocrystalline Alloys from Amorphous Precursors, NATO Science Series II: Mathematics, Physics and Chemistry, vol. 184, Kluwer Academic Publishers, Dordrecht, 2005, pp. 79–90.